Aerosol-assisted Atmospheric Cold Plasma Deposition and Characterization of Superhydrophobic Organic-Inorganic Nanocomposite Thin Films

Fiorenza Fanelli,,† Anna M. Mastrangelo,‡ and Francesco Fracassi‡,†*

†Institute of Inorganic Methodologies and Plasmas, National Research Council (IMIP-CNR), c/o Department of Chemistry, University of Bari Aldo Moro, via Orabona 4, 70126 Bari, Italy

‡Department of Chemistry, University of Bari Aldo Moro, via Orabona 4, 70126 Bari, Italy

ABSTRACT

A facile atmospheric pressure cold plasma process is presented to deposit a novel organic-inorganic hydrocarbon polymer/ZnO nanoparticles nanocomposite coating. Specifically, this method involves the utilization of an atmospheric pressure dielectric barrier discharge (DBD) fed with helium and the aerosol of a dispersion of oleate-capped ZnO nanoparticles (NPs) in n-octane. As assessed by X-ray photoelectron spectroscopy (XPS) and attenuated total reflectance-Fourier transform infrared (ATR-FTIR) spectroscopy, the deposited nanocomposite coating combines the chemical features of both the oleate-capped ZnO NPs and the polyethylene-like organic component originated from the plasma-polymerization of n-octane. Additionally, scanning electron microscopy (SEM) and transmission scanning electron microscopy (TSEM) confirm the synthesis of hierarchical micro/nanostructured coatings containing quasi-spherical NPs agglomerates. The polyethylene-like polymer covers the NPs agglomerates to different extents and contributes to their immobilization in the three-dimensional network of the coating. The increase of both the deposition time (1 - 10 min) and the NPs concentration in the dispersion (0.5 – 5 wt %) has a significant effect on the chemical and morphological structure of the thin films and, in fact, results in the increase the ZnO NPs content, which ultimately leads to superhydrophobic surfaces (advancing and receding water contact angles higher than 160°) with low hysteresis due to the hierarchical multiscale roughness of the coating.

1. INTRODUCTION

Intense research efforts are directed nowadays towards the development of new synthetic strategies for the preparation organic/inorganic nanocomposite (NC) thin films consisting of polymers and inorganic nanoparticles (NPs) with size generally smaller than 100 nm. According to previous research, among different properties, these coatings can exhibit superhydrophobic behavior (i.e., water contact angle greater than 150° and contact angle hysteresis less than 10°) due to the combination of a low surface energy organic component and an adequate surface roughness induced by NPs incorporation.[1-2]

Recently aerosol-assisted processes have been widely utilized for the preparation of this class of NC coatings; in their simplest form these processes exploit the atomization of a dispersion of preformed NPs in a suitable solvent. Interestingly, organic-inorganic NC coatings with a hierarchical microscale-to-nanoscale nanotextured surface morphology can be produced by the simple spray-deposition (also referred to as spray-casting) of a dispersion of NPs and a preformed organic polymer, typically followed by air-drying under ambient condition or by mild heat treatment to remove any solvent residual and cure the coating.[3-5] For instance, perfluoroacrylic polymer/ZnO NPs nanocomposite coatings were obtained by Steele et al.[4] from suspensions of fluoroalkyl methacrylic copolymer and ZnO NPs in water, using acetone as a proper cosolvent. Noticeably, alternative strategies are the spray-deposition of a dispersion containing the NPs and the organic precursors of the polymeric component, followed by thermal or photoinduced polymerization of the precursors.[6,7] In a recent example, Sparks et al.[6] reported the production of a NC coatings via spray-casting of a dispersion containing SiO_2 nanoparticles, UV-curable resin (i.e., thiol-ene resin), a photoinitiator and a low boiling point organic solvent, followed by photopolymerization to afford the organic matrix formation. It was shown that the

combination of the spray-deposition process and NPs dispersion/agglomeration provides surfaces with hierarchical morphology and superhydrophobic character. Interestingly, the aerosol-assisted chemical vapor deposition (AACVD) has demonstrated to be a facile single-step strategy towards NC coatings;[8,9] in this process the aerosol of a dispersion of NPs is transported by a carrier gas to a reactor (either hot-wall or cold-wall reactor) where a heated substrate is located. Due to the high operating temperatures, most published studies on this strategy refer to the production of inorganic NC coatings in which for instance the inorganic NPs are embedded in a host metal oxide matrix.[8,9] However, very recently it was shown that the adequate choice of the organic component and of the temperature, allows avoiding the pyrolytic decomposition of the organic fraction and affords the deposition of organic-inorganic NC coatings. Crick et al.[10,11] incorporated preformed NPs into a polydimethylsiloxane (PDMS) polymer using a cold-walled AACVD technique. They atomized a chloroform suspension of a thermosetting silicone elastomer, containing a curing agent, and NPs adequately functionalized with a surfactant. While the NPs were functionalized to be readily dispersible in chloroform, the curing agent was added to promote crosslinking and hardening of the polymer, and therefore to generate a heat resistant organic matrix. It was observed that the elastomer cures around NPs agglomerates forming PDMS bulbs that protrude from the surface and are responsible of both microstructure and superhydrophobic character of the coatings.

Here we report, for the first time, the deposition of superhydrophobic organic-inorganic NC coatings by aerosol-assisted atmospheric cold plasma deposition. This process can be considered as a variation of the classical AACVD in which the atmospheric plasma, fed with a carrier gas and the aerosol of a dispersion of NPs in a liquid organic precursor, allows the deposition in a

single step and at room temperature of an organic-inorganic NC coating; the NPs are embedded in the organic matrix formed by the plasma-polymerization of the organic precursor.[12-17] Specifically, in this work polyethylene-like polymer/zinc oxide nanoparticles NC films were produced, the utilization of ZnO NPs being intended for future photocatalytic and self-cleaning applications of the deposited coatings. First, commercial ZnO NPs were appropriately compatibilized by surface-functionalization with oleate; then, a dielectric barrier discharge (DBD) fed with helium and the aerosol of a dispersion of oleate-capped ZnO NPs in n-octane (i.e., the hydrocarbon liquid precursor) was utilized to deposit the NC coatings. To clarify how the hydrocarbon polymeric fraction and the ZnO NPs organize in the plasma-deposited NC, the growth and structure of the thin films were investigated as a function of the deposition time and of the NPs concentration in the dispersion. The coatings contain quasi-spherical NPs agglomerates which promote the formation of a hierarchical surface roughness that ultimately leads to superhydrophobic surfaces with low hysteresis. To our best knowledge of previous research on organic-inorganic NC coatings produced by aerosol-assisted atmospheric cold plasma deposition,[13-17] the present study provides the first example evidencing this kind of hierarchical surface texture and wettablity behavior.

2. EXPERIMENTAL SECTION

Chemicals. ZnO nanoparticles (99.5%) with average particle size of 36 nm, nearly spherical shape and hexagonal crystal structure were purchased from ABCR GmbH & Co. KG. Oleic acid (*cis*-9-octadecenoic acid, 90%), ethanol (absolute, ≥99.8%) and n-octane (>99%) were purchased by Sigma-Aldrich and utilized without further purification. Deionized water, sodium

hydroxide (NaOH, 98%, Sigma-Aldrich), nitric acid (HNO_3, 65%, Sigma-Aldrich), perchloric acid ($HClO_4$, 70%, Sigma-Aldrich) and acetate buffer solution (Fluka) were also utilized.

Preparation of oleate-capped ZnO nanoparticles. The surface of commercial ZnO nanoparticles was functionalized with oleate according to the following procedure: 10 mL of a 1.0 M aqueous NaOH solution were added to 10 mL of a 0.60 M aqueous solution of oleic acid under continuous stirring, then 2.0 g of ZnO NPs were dispersed in the resulting solution and, finally, 20 mL of deionized water were added. The resulting mixture was allowed to react under vigorous stirring at 60 ºC for a total reaction time of 20 hours. After reaction completion, the mixture was centrifuged, the resulting nanoparticles were isolated, washed and centrifuged twice with ethanol (5 mL) and finally dispersed in n-octane.

Deposition of nanocomposite thin films. Nanocomposite thin films were deposited in the atmospheric pressure plasma reactor with dielectric barrier discharge (DBD) configuration shown in Figure S1 of the Supporting Information. The plasma is generated between two parallel plate electrodes (4 mm gas gap, 50x50 mm^2 electrode area) both covered with a 0.635 mm thick Al_2O_3 plate (CoorsTek, 96%), by applying a sinusoidal AC high voltage (26 kHz, 2 kV_{rms}) by means of a STT Calvatron power supply (model SG2) operated in pulsed mode (20 ms period, 13 ms plasma on-time, 65% duty cycle). Under these conditions the average specific power dissipated in the DBD was equal to 0.28 ± 0.02 $W \cdot cm^{-2}$. Each electrode consisted of a Ag-Pd metallization layer directly realized on the Al_2O_3 plate. The DBD electrode system was located into a Plexiglas chamber (volume of about 14 L) slightly pumped with a dry diaphragm pump (Pfeiffer), to keep the working pressure constant (10^5 Pa) as measured by a MKS capacitive pressure gauge. During the deposition process the atmospheric plasma was fed by He (Airliquide, 99.999%) and the aerosol of a dispersion of oleate-capped ZnO NPs in n-octane, at a

concentration ranging from 0.5 to 5 wt %. The feed mixture was introduced in the discharge zone through a slit and pumped through a second slit positioned on the opposite side (longitudinal gas injection). The total He flow rate was equal to 8000 sccm; a fixed He flow rate of 2800 sccm was utilized for the operation of a pneumatic atomizer (TSI, model 3076) and allowed the atomization of the dispersion at a mass flow rate of 0.23 ± 0.02 g·min^{-1}. The dispersion was sonicated for 2 h before each experiment and kept under continuous magnetic stirring during atomization. The gas flow rates were controlled with MKS mass flow controllers (MFC), while the effective amount of dispersion atomized per unit time was evaluated by weight variation per unit time of the dispersion reservoir. Before each experiment, the Plexiglas chamber was purged with 8000 sccm of He for 10 min to remove air contaminations. The deposition processes duration (deposition time, t_d) was varied between 1 and 10 min. Thin films were deposited on substrates (i.e., borosilicate glass slides, CaF_2 substrates, carbon-coated Cu grids) located in the middle of the DBD region on the lower electrode.

ZnO nanoparticles and thin films characterization. X-ray Photoelectron Spectroscopy (XPS) analyses were performed using a Thermo Electron Theta Probe spectrometer equipped with a monochromatic Al Ka X-ray source (1486.6 eV) operated at a spot size of 300 μm corresponding to a power of 70 W. Survey (0–1200 eV) and high resolution (C1s, O1s, and Zn2p) spectra were recorded in FAT (fixed analyzer transmission) mode at pass energy of 200 and 100 eV, respectively. All spectra were acquired at a take-off angle of 37° with respect to the sample surface. A flood gun was used to balance the surface charging. Charge correction of the spectra was performed by taking the hydrocarbon (C-C/C-H) component of the C1s spectrum as internal reference (binding energy, BE = 285.0 eV).[18] Atomic percentages were calculated from the high resolution spectra using the Scofield sensitivity factors set in the Thermo Avantage software

(Thermo Fisher Corporation) and a non-linear Shirley background subtraction algorithm. The analyses were repeated on three samples produced in different experiments. The best-fitting of the high-resolution C1s and O1s spectra was performed using the Thermo Avantage software; the full-width at half maximum (FWHM) of each C1s and O1s lineshape was allowed to vary between 1.3 - 1.7 eV and a maximum relative standard deviation of 10% was estimated on the area percentages of the curve-fitting components.

A vacuum Fourier transform infrared (FTIR) spectrometer was used to register the infrared absorption spectra (375 – 4000 cm^{-1} range, 4 cm^{-1} resolution) of NPs and of thin films deposited on CaF_2 substrates (Crystran, 0.5 mm thickness). Spectra were collected in attenuate total reflectance (ATR) mode utilizing an ATR module equipped with a single reflection diamond ATR crystal (refractive index of 2.4). NPs and thin film ATR-FTIR spectra, obtained after subtraction of the CaF_2 substrate spectrum, were baseline corrected and normalized to the most intense absorption band. FTIR spectra were also collected in transmission mode for pristine and oleate-capped ZnO nanoparticles.

The ZnO loading in the NC coating, defined as weight percentage (wt %) of ZnO, was determined by anodic stripping voltammetry (ASV) using a Metrohm 757 VA Computrace polarograph. A weighed amount of NC coating was deposited by DBD on borosilicate glass substrate, then the coating was dissolved using a wet digestion procedure with nitric-perchloric acids. Electrochemical determination of dissolved zinc was performed in differential pulse ASV mode using a classical 3-electrode cell provided with a hanging mercury drop electrode (HMDE) used as the working electrode, an Ag/AgCl with saturated 3 M KCl reference electrode and a platinum wire counter electrode. The solutions obtained after digestion were diluted with deionized water, adjusted to pH of 5.0-5.5 with acetate buffer solution, and deaerated with a

stream of nitrogen for 100 s. Electrochemical deposition was performed at -0.8 V for 45 s under stirring. After this time the stirrer was switched off and the oxidation curves were recorded in the potential range from -1.15 to -0.75V (sweep rate of 0.06 $V \cdot s^{-1}$). Zinc was quantified by addition of a Zn^{2+} standard solution in the cell. As known amounts of coatings were dissolved, the loading of ZnO was straightforward. The reported loading values are the average of three measurements on six different samples produced in different experiments. An analogous procedure was utilized for determination of ZnO loading in the oleate-capped ZnO NPs.

The thickness of coatings deposited on 0.15 mm thick borosilicate glass substrates was estimated using an Alpha-Step 500 KLA Tencor Surface profilometer. Measurements were repeated on three different samples produced in different experiments and a relative standard deviation of 30% was associated to average thickness values due to the high surface roughness of the NC coatings and to the fact that the penetration of the profilometer tip in the coatings cannot be ruled out. The deposition rate was calculated by dividing the average film thickness by the deposition time.

The morphology of the plasma-deposited films and of the ZnO nanoparticles (pristine and oleate-capped NPs) was investigated by a Zeiss SUPRA™ 40 field emission scanning electron microscope (FESEM). SEM images were acquired with a high resolution in-lens secondary electron detector at the working distance of 2 mm and electron acceleration voltage (extra-high tension, EHT) of 2 kV (unless otherwise specified), magnification in the range 5 - 500 kx. Thin films deposited by DBD on borosilicate glass substrates were sputter-coated with a 10 nm thick layer of Cr prior to SEM observation utilizing a turbo-pumped sputter coater (Quorum Technologies, model Q150T); cross-sectional SEM analyses were carried out after samples fracturing with tweezers. For SEM observation, pristine and oleate-capped ZnO nanoparticles

were dispersed in water and n-octane, respectively, then ultrasonicated for 2 hours, drop-casted (5 μl drop) on small pieces of a c-Si(100) substrates, and analyzed after solvent evaporation at room temperature (no sample metallization). Size distribution of NPs agglomerates in the nanocomposite coatings was estimated by SEM images with the help of a dedicated software (Image J). The morphological investigation was also performed utilizing the multimode transmission scanning electron microscopy (TSEM) detector of the Zeiss SUPRA™ 40 FESEM both in bright-field (BF) and dark-field (DF) modes, at EHT of 20 and 30 kV, working distance in the range 1.5 - 2.2 mm, magnification ranging between 5 kx and 500 kx. TSEM analyses of NPs were performed after drop-casting of a 5 μl drop of a NPs dispersion onto carbon-coated 300 mesh copper grids with a procedure similar to that utilized for the preparation of SEM samples; TSEM analyses were also carried out on NC coatings directly deposited for 2 min onto carbon-coated copper grids.

Atomic force microscopy (AFM) was utilized to determine the route mean square (RMS) surface roughness of the coatings. Analyses were carried out with a Park System XE-70 microscope in non-contact mode using Nanosensors PPP-NCHR tips with resonance frequency of ~280 kHz. The reported RMS roughness values are the mean of the three measurements on different samples over 20 x 20 μm^2 surface areas.

Surface wettability was evaluated with a Ramé-Hart manual goniometer (model 100) by dynamic water contact angle (WCA) measurements using the sessile drop method in order to assess advancing and receding contact angles (θ_A and θ_R, respectively) and to estimate the contact angle hysteresis, CAH (difference between θ_A and θ_R). A dropl of 1 μl in volume was at first deposited on the sample surface by a micrometer syringe and its volume was increased forcing the drop to advance on the sample. Advancing angles were the maximum angles

observed during the droplet growth. Then the drop was progressively shrunk, receding contact angles were the ones just before the contact surface reduction. The reported WCA values are the average of measurements on three different samples produced in different experiments (five measurement for each sample) with an estimated maximum error of 3°.

The adhesion of the coatings to glass substrates was tested using a Scotch 810 Magic Tape (3M) based on the ASTM standard (D3359).[19,20] In this peel test, the tape was pressed against the coating with a fingertip and after 60 s it was pulled off rapidly back at an angle as close as possible to 180°. WCA measurements and SEM analyses were performed before and after the tape adhesion test. The reported WCA values are the average of measurements on three different samples (five measurement for each sample).

3. RESULTS AND DISCUSSION

DBDs fed by He and the aerosol of pure n-octane (mass flow rate = 0.23 ± 0.02 g·min^{-1}) allowed the synthesis of smooth and uniform thin films (RMS roughness of 0.345 ± 0.007 nm) at a deposition rate of 19 ± 3 nm·min^{-1}. The ATR-FTIR spectrum of the coating in Figure 1 is characterized by the typical absorption features of a polyethylene-like (PE-like) polymer, i.e., the band of sp^3 C-H stretching in the range 2800 – 3000 cm^{-1}, and the bending of sp^3 CH_2 and CH_3 groups at 1461 cm^{-1} and 1377 cm^{-1}, respectively.[21] Results from XPS analysis (Table 1) indicate a very low oxygen surface atomic concentration (2.0 ± 0.5%) reasonably ascribable to oxygen and water vapor contaminations in the Plexiglas chamber of the DBD reactor and/or to oxygen uptake upon post-deposition air exposure of the coating. The high-resolution C1s XPS spectrum of the coating (Figure 2a) can be curve-fitted with the dominant aliphatic hydrocarbon

component (C-C/C-H) at 285.0 ± 0.2 eV and the weak peak due to C-O groups at 286.5 ± 0.2 eV (about 2% peak area).[18]

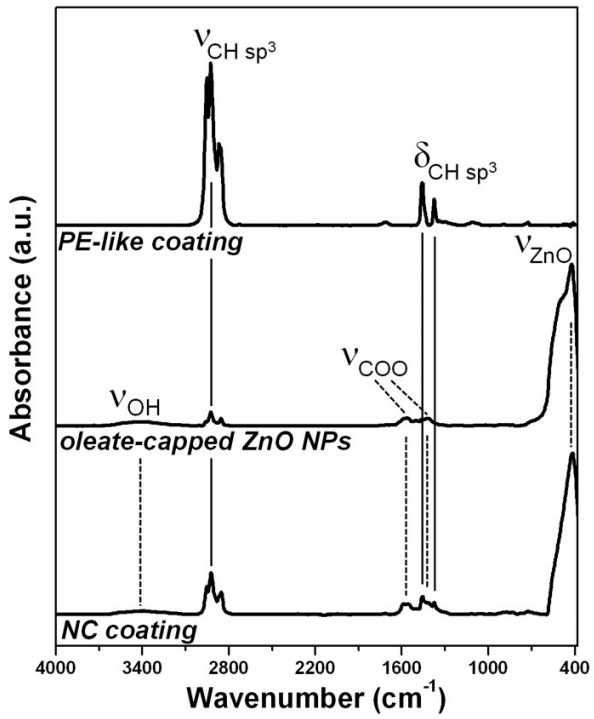

Figure 1. FTIR spectra of (a) polyethylene-like coating deposited for 10 min in a DBD fed with He and the aerosol of n-octane (ATR mode), (b) oleate-capped ZnO NPs (transmission mode), (c) NC coating deposited for 10 min in a DBD fed with He and the aerosol of a 3 wt % oleate-capped ZnO NPs dispersion in n-octane (ATR mode).

Table 1. XPS surface atomic concentrations: (a) polyethylene-like coating deposited for 10 min in a DBD fed with He and the aerosol of n-octane; (b) oleate-capped ZnO NPs; (c) nanocomposite film deposited for 10 min in a DBD fed with He and the aerosol of a 3 wt % oleate-capped ZnO NPs dispersion in n-octane.

		C%	O%	Zn%
a	PE-like coating (n-octane)	98.0 ± 0.5	2.0 ± 0.5	--
b	Oleate-capped ZnO NPs	55 ± 4	29 ± 2	16 ± 2
c	NC coating (3 wt % oleate-capped ZnO NPs dispersion in n-octane)	87 ± 3	10 ± 3	3.0 ± 0.5

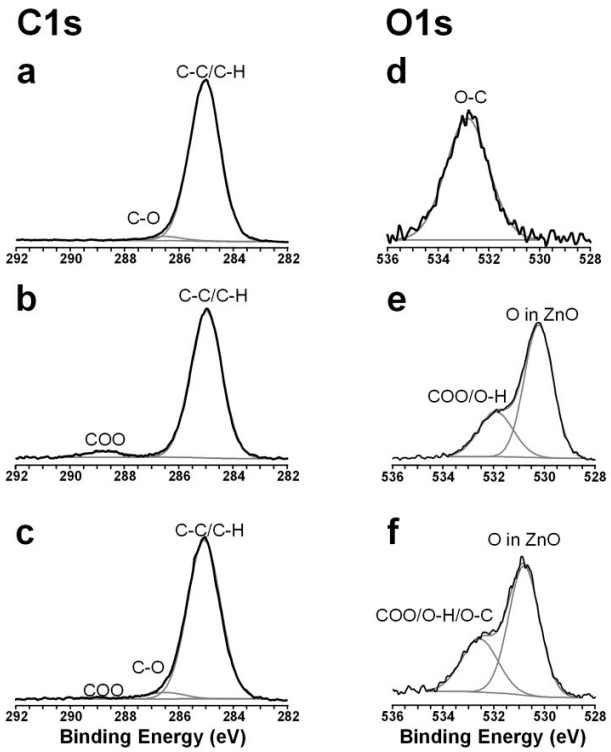

Figure 2. High resolution XPS C1s and O1s spectra: (a, d) polyethylene-like coating deposited in a DBD from n-octane aerosol (deposition time = 10 min), (b, e) oleate-capped ZnO NPs, (c, f) nanocomposite coating deposited in a DBD from a 3 wt % oleate-capped ZnO NPs dispersion in n-octane (deposition time = 10 min).

The dispersion of commercial ZnO NPs in n-octane was highly unstable since, even under ultrasonication and stirring, the inorganic polar NPs tended to separate from the organic non-polar solvent and precipitate. For this reason, ZnO NPs were first successfully surface-functionalized with oleate (capping), according to the procedure described in the experimental section, and then appropriately dispersed in n-octane. The FTIR spectrum of the oleate-capped ZnO NPs in Figure 1 displays the intense ZnO stretching band (maximum at about 420 cm^{-1}),[22,23]

the broad band centered at about 3400 cm^{-1} related to the OH stretching of hydroxyl groups on the ZnO NPs surface and/or adsorbed water vapor, the typical CH_x stretching signals due to the oleate in the range 2800 – 3050 cm^{-1} (Supporting information, Figures S2 and S3) and two absorptions ascribed to the asymmetric and symmetric stretching of the oleate carboxylate group at 1566 cm^{-1} and 1418 cm^{-1}, respectively.[24-27] The wavenumber separation between the COO bands (148 cm^{-1}) indicates that the carboxylate group of the oleate molecule very likely interacts with the Zn atoms on the ZnO NPs surface via a bridging bidentate coordination mode (Supporting information, Section SI2).[24-27] The quantitative XPS analysis of the oleate-capped NPs shows a surface carbon atomic percentage of 55 ± 4% (Table 1). The high-resolution C1s spectrum in Figure 2b is curve-fitted with the C–C/C-H (285.0 ± 0.2 eV) and COO (288.8 ± 0.2 eV) components and, in good agreement with the theoretical percentages of aliphatic and carboxylate C atoms in the oleate molecule (94.4% aliphatic C : 5.6% carboxylic C), the peak area percentage ascribed to carboxylate was 5%. The $Zn2p_{3/2}$ XPS signal of the oleate-capped NPs is symmetrical and centered at 1021.6 eV, as reported for ZnO[28-30] and also observed in the case of the pristine NPs; while the O1s spectrum (Figure 2e) displays two components associated to oxygen in ZnO structure (530.2 ± 0.2 eV, 72%) and to oxygen in carboxylate and hydroxyl groups (531.9 ± 0.2 eV, 28%).

The nanocomposite coating, deposited for 10 min in a DBD fed with He and the aerosol of a 3 wt % oleate-capped ZnO NPs dispersion in n-octane, showed the chemical features of both the oleate-capped ZnO NPs and the organic component due to the plasma-polymerization of n-octane. In fact, the ATR-FTIR spectrum in Figure 1 is characterized by the absorption bands due to ZnO (420 cm^{-1}), the OH stretching band (3400 cm^{-1}), the COO asymmetric and symmetric stretching signals (in the range 1300-1600 cm^{-1}) ascribed to the oleate-capped ZnO NPs, while

the CH_2 and CH_3 stretching and bending signals (2800-3000 cm^{-1} and 1300-1600 cm^{-1}, respectively) show good agreement with the corresponding bands observed in the case of the polyethylene-like coating deposited from a pure n-octane aerosol. No appreciable olefinic CH signals (e.g., the signal ascribed to the =C–H symmetric stretching in oleate at 3005 cm^{-1}) were detected. This fact does not represent unequivocal evidence for reaction of the C=C bond of the oleate molecules, because it could simply indicate that the concentration of C=C double bonds in the NC coating is reduced below the detection limit of ATR-FTIR due to dilution of the polyethylene-like polymer, without any chemical reaction.

As reported in Table 1, the nanocomposite coating is characterized by a higher XPS C atomic percentage (87 ± 3%) than the oleate-capped ZnO NPs, while lower percentages are detected for Zn and O (10 ± 3% and 3.0 ± 0.5%, respectively). The high-resolution C1s spectrum (Figure 2c) is dominated by the hydrocarbon component and shows very weak peaks due to C-O (5%) and COO (< 1%). The $Zn2p_{3/2}$ signal is symmetrical and slightly shifted towards higher BE (1022.2 ± 0.2 eV) with respect to the oleate-capped NPs. Both FTIR and XPS results confirm that zinc oxide keeps its chemical integrity in the NC coating. The high-resolution O1s peak of the NC coating in Figure 2f is curve-fitted with the peak ascribed to oxygen in ZnO (66%) and to oxygen in COO, OH and CO (34%). It is worth highlighting that this NC coating deposited from a 3 wt % dispersion of oleate-capped NPs in octane exhibits a ZnO loading of 68 ± 5 wt % evaluated by ASV measurements after coating digestion.

As shown in Figure 3a, the nanocomposite coating consists of NPs agglomerates which seem to be covered at different extents by the organic component originated from the plasma-polymerization of n-octane. NPs agglomerates present mean diameter of 640 nm (minimum and maximum size of about 250 and 2200 nm, respectively), nearly lognormal size distribution with

a geometric standard deviation (σ_G) of 2 in agreement with typical polydisperse aerosol population reported for the pneumatic atomizer utilized in this work (Supporting Information, Figure S5). This coating has RMS roughness of 574 ± 11 nm.

Figure 3 compares the SEM images of the nanocomposite coatings to those obtained from drop-casting and spray-deposition of the oleate-capped ZnO NPs dispersion on a c-Si substrate. Figures 3d and 3e clearly show NPs aggregates of irregular size and dimension deposited on a c-Si substrate by drop-casting of the dispersion (TSEM images are reported in the Supporting Information, Figure S6). While, as reported for spray-drying of dispersions of preformed NPs,[32,33] the spray-deposition results in NPs aggregates which very often exhibit a quasi-spherical shape (Figures 3g and 3h). These quasi-spherical aggregates are detected also in the plasma-deposited coating, and, as evident in the high magnification images of Figures 3b and 3c, they seem to be coated by a thin layer (i.e. the organic component due to plasma-polymerization) which is not observed in case of analogous aggregates collected by simply atomizing the dispersion (Figures 3h and 3i). As evident from the TSEM images (Supporting Information, Figure S6), in the nanocomposite coatings the NPs seem to be more densely packed in the agglomerates than in the case of the drop-casted dispersion.

This evidence supports the hypothesis that a certain n-octane evaporation occurs at the aerosol droplets surface, and therefore the NPs (or the NPs aggregates) undergo evaporation-induced agglomeration to form locally closely-packed structures. Analogous results are widely reported and discussed in the scientific literature on aerosol-assisted processes utilizing the atomization of a liquid dispersion containing NPs towards the production of nanostructured and nanocomposite thin films.[3-7,11,34,35]

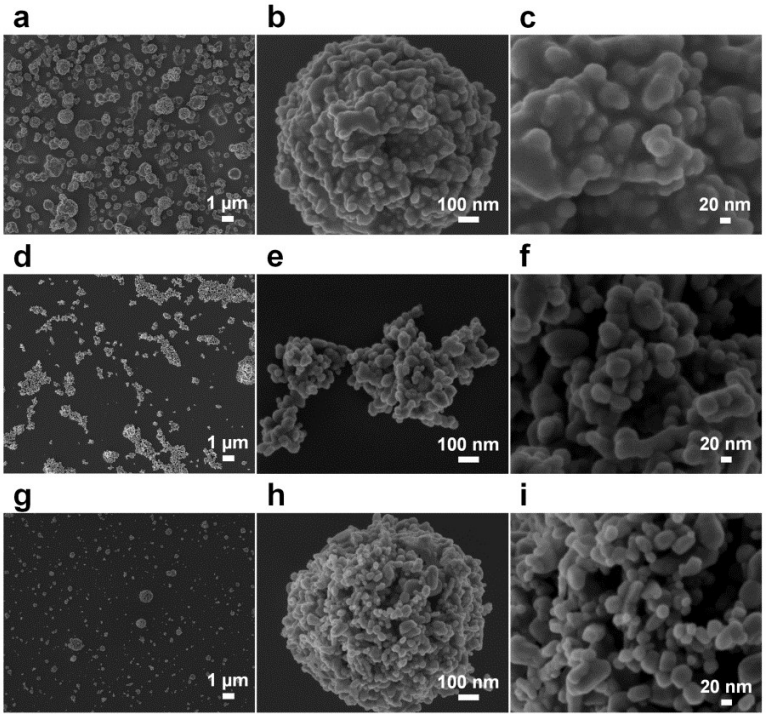

Figure 3. SEM images: (a, b, c) NC coating deposited for 10 min in a DBD fed with He and the aerosol of a 3 wt % oleate-capped ZnO NPs dispersion in n-octane, (d, e, f) sample obtained from drop-casting of the NPs dispersion on a c-Si substrate; (g, h, i) sample obtained collecting the aerosol of the NPs dispersion on a c-Si substrate.

The presence of a thin layer of hydrocarbon polymer covering the NPs agglomerates is evidenced in Figure 4 which compares the SEM, the bright-field TSEM, and the dark-field TSEM images of a typical spherical agglomerate acquired at an electron acceleration voltage of 20 kV. Specifically, the SEM image (Figure 4a) evidences the surface of the agglomerate covered by the polymeric layer, however due to the high electron accelerating voltage utilized for image acquisition, and hence the deeper penetration of the electrons and larger interaction volume,[36] only the general surface profile of the agglomerate can be distinguished; surface details can be clearly observed at lower electron acceleration voltages as in Figures 3b and 3c, showing the SEM image of a NPs agglomerate recorded at the electron acceleration voltage of 2

kV. The bright-field TSEM image (Figure 4b) is dominated by the mass-thickness contrast,[37] and therefore shows a dark agglomerate due to the scattering of electrons to higher angles than the acceptance angle of the bright-field detector. The dark-field TSEM image of Figure 4c, better evidences the presence of NPs in the agglomerate. Indeed, the high magnification dark-field TSEM image in Figure 4d allows the estimation of the thickness of the organic layer on the agglomerate (between 10 and 20 nm, in this image). The dark-field TSEM mode is particularly suitable to distinguish the organic and the inorganic components of the nanocomposite because it utilizes an off-axis annular detector able to collect only scattered electrons and, therefore, more sensitive to small variations in sample properties.[37] In dark-field mode both the mass-thickness contrast and the Z-contrast (i.e., related to the atomic number) contribute to image formation,[37] and, as a consequence, in the present study this TSEM mode allows better discriminating the inorganic component from the organic component due to the fact that Zn has the highest atomic number in the nanocomposite.

It is worth mentioning that neither SEM nor TSEM observations permitted to reveal the presence of the oleate layer on the surface of the oleate-capped ZnO NPs, likely due to the fact that the thickness of this organic layer is very low. Therefore, even if the reaction of the oleate molecule on the NPs surface during the plasma process cannot be excluded, it seems reasonable to assume that the organic layer covering the NPs agglomerates in the nanocomposite coating (e.g., Figures 3 and 4) can be predominantly ascribed to the plasma-polymerization of n-octane. This hypothesis is supported by the evidence that the surface morphology of the oleate-capped NPs agglomerates, purposely collected on a glass substrate by spray-deposition, does not change after exposure to a pure He DBD under the same experimental conditions utilized in this work (SEM images in the Supporting Information , Figure S7).

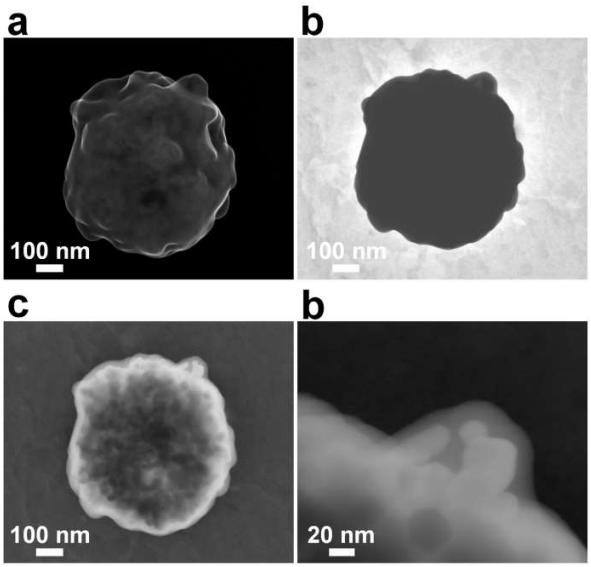

Figure 4. (a) SEM, (b) bright-field TSEM, (c) dark-field TSEM images of a typical agglomerate (EHT = 20 kV); (d) high-magnification dark-field TSEM image evidencing the organic layer on the NPs agglomerate.

The growth and structure of the NC coating was investigated as a function of the deposition time with a dispersion at a NPs concentration of 3 wt % in n-octane. Figure 5a shows that with increasing the deposition time, the relative intensity in the ATR-FTIR spectra of the CH_x absorption features decreases with respect to that of ZnO, while SEM images in Figure 5b clearly display the increase of the NPs agglomerates density as a function of the deposition time. The Zn XPS atomic concentration varies from 1.0 ± 0.4% at 1 min to 3.0 ± 0.5% at 10 min. This quite slight variation of the Zn XPS percentage, respect to the important change of FTIR spectra and agglomerates density in Figure 5, can be ascribed to the fact that, since XPS has a maximum sampling depth of about 10 nm, the surface composition of the NC coating as determined by XPS is very likely dominated by the organic layer which covers the NPs agglomerates.

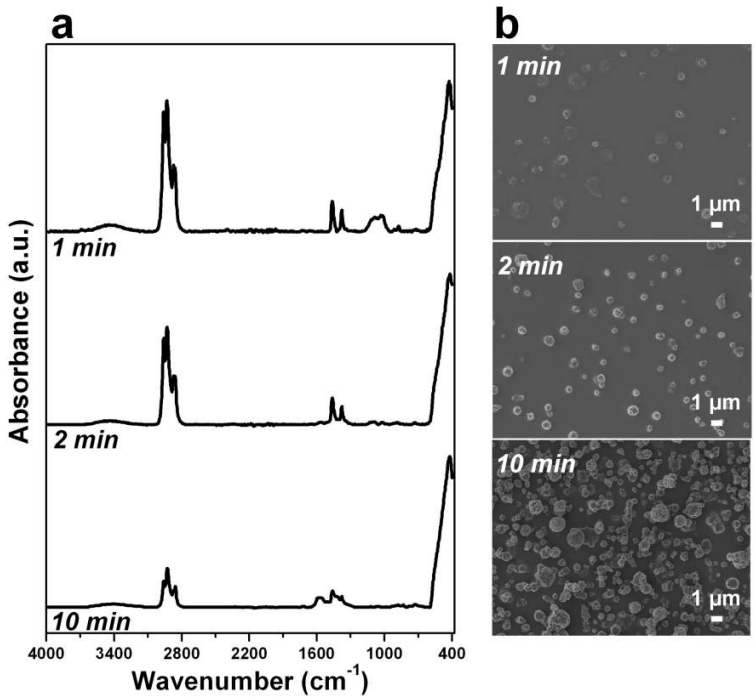

Figure 5. (a) ATR-FTIR spectra and (b) SEM images of NC films deposited by DBD from a 3 wt % oleate-capped ZnO NPs dispersion in n-octane as a function of the deposition time (1, 2 and 10 min).

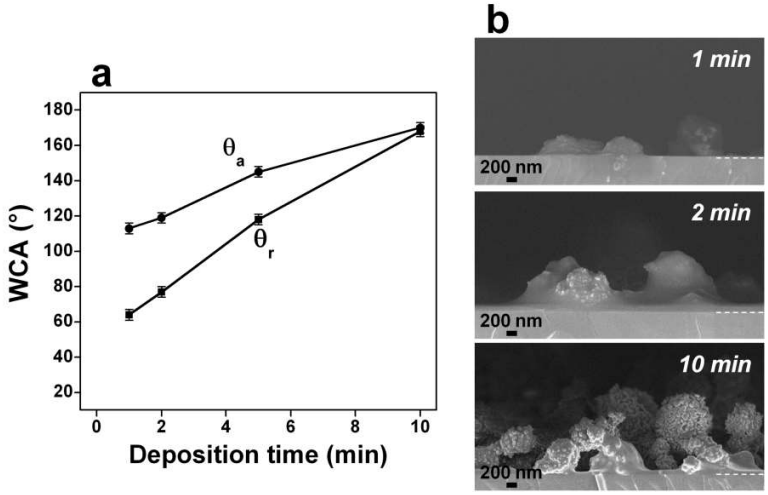

Figure 6. (a) Advancing and receding WCAs of the NC coatings versus the deposition time (3 wt % oleate-capped ZnO NPs dispersion in n-octane); (b) cross-sectional SEM images of NC films deposited at different deposition times (1, 2 and 10 min).

The deposition time significantly affects the wettability of the coating, and in fact, as shown in Figure 6a, with increasing the deposition time from 1 to 10 min, advancing (θ_a) and receding (θ_r) contact angles increase from 113° to 170° and from 64° to 168°, respectively. Therefore, superhydrophobic surfaces (θ_a and θ_r greater than 150°) with very low hysteresis were produced at 10 min deposition time. Noticeably, a polyethylene-like coating deposited by a DBD fed with n-octane aerosol for 10 min shows advancing and receding WCA values equal to 106° and 95°, respectively. The wetting behavior of the NC coating can be ascribed to the presence of a hydrocarbon polymer component with a low surface energy and of NPs agglomerates which generate a hierarchical multiscale morphology,[3,32] as clearly evidenced by the cross-sectional SEM images in Figure 6b. NPs agglomerates provide the micrometer-scale roughness, while the NPs on top of the agglomerates provide the nanoroughness. Such NPs organization in a hierarchical (i.e., microscale-to-nanoscale) morphology is known to produce superhydrophobicity and low contact angle hysterises.[2-4,6,38] In particular, the appearance of a hierarchical roughness as a function of the deposition time produces the transition from a Wenzel state (complete wetting) characterized by high values of CAH and, therefore, water droplet adhesion to the surface, to a Cassie-Baxter state (partial wetting) in which water droplets sit partially on top of surface protrusions and exhibit small CAH.[2-4,6,38] It is worth highlighting that thin films deposited for 10 min from pure n-octane and from a 3 wt % NPs dispersion in n-octane are characterized by RMS roughness values of 0.345 ± 0.007 nm and 574 ± 11 nm, respectively.

The increase of the concentration of the ZnO NPs in the dispersion from 0.5 to 5 wt % resulted in a higher ZnO loading in the coatings (from 19 ± 3 wt % to 78 ± 4 wt %, Figure 7a), as also

confirmed by the increase of the intensity ratio between the ZnO and the CH_x absorption bands in the ATR-FTIR spectra (Figure 7b). Accordingly, XPS results show an increase of the Zn atomic surface concentration from less than 0.5% to 4.5 ± 0.7% and a concomitant decrease of the C atomic concentration from 99 ± 2% to 85 ± 3%.

SEM images in Figure 7c show that the coating deposited from a 0.5% wt % NPs dispersion has a smooth morphology (RMS roughness of 6.1 ± 1.4 nm) dominated by the polyethylene-like component and presents few NP aggregates; this coating, in fact, is produced at the same deposition rate observed for the polyethylene-like thin film from pure n-octane aerosols. The dark-field TSEM images (Supporting Information, Figures S8a and S8b) evidence also the presence of a few non-agglomerated NPs in the coating. With increasing the NPs concentration in the dispersion, the number of NPs agglomerates in the coating increases (Figure 7b) along with the RMS roughness (Figure 8a) and the average thickness of the coating, as demonstrated by the cross-sectional SEM images in Figure 8b (the deposition rate with a 5 wt % ZnO dispersion was about 110 $nm \cdot min^{-1}$). TSEM analyses allow the presence of unagglomerated NPs in the polymeric matrix to be excluded at a NPs concentration higher than 3 wt % (Supporting Information, Figures S8c and S8d). Furthermore no significant change of the NPs agglomerate size distribution can be observed as a function of the NPs concentration in the dispersion. As expected, the increase of the NPs content in the dispersion and in the coating (and therefore of the surface RMS roughness) results in a steep increase of both the advancing and receding WCAs at NPs concentration in the dispersion higher than 2 wt % (Figure 8c). Specifically, at NPs concentration lower or equal than 2 wt % the maximum values for advancing and receiding contact angles are 117° and 93°, respectively, with a maximum hysteresis of about 30°; while at higher NPs concentrations superhydrophobic surfaces are obtained characterized by θ_a and θ_r

greater than 160° and hysteresis lower than 8°. This trend can be clearly ascribed to the fact that as the NPs content increases, a transition from a polymer-dominated to a nanoparticles-dominated surface morphology occurs (Figure 8b) due to the abundant inclusion of NPs agglomerate in the coating.

The deposited coatings stored under ambient conditions retain their chemical structure, morphology and superhydrophobic character over long-term storage under ambient conditions (aging tests carried out after storage for 24 months).

To assess whether the NC coatings adhere to the substrate, the tape peel test was performed on thin films deposited on glass substratesfrom a 3 wt % NPs dispersion. Briefly, the results demonstrated that while a certain fraction of NPs agglomerates is removed (in particular larger agglomerates), the hydrocarbon polymer layer at the NC coatings/substrate interface robustly adhere to the substrate (SEM images in Figure S9). WCA measurements carried out with increasing the thickness of the coating indicated that an average thickness of about 1000 nm is required to keep low hysteresis superhydrophobic surfaces after the test (Figure S10).

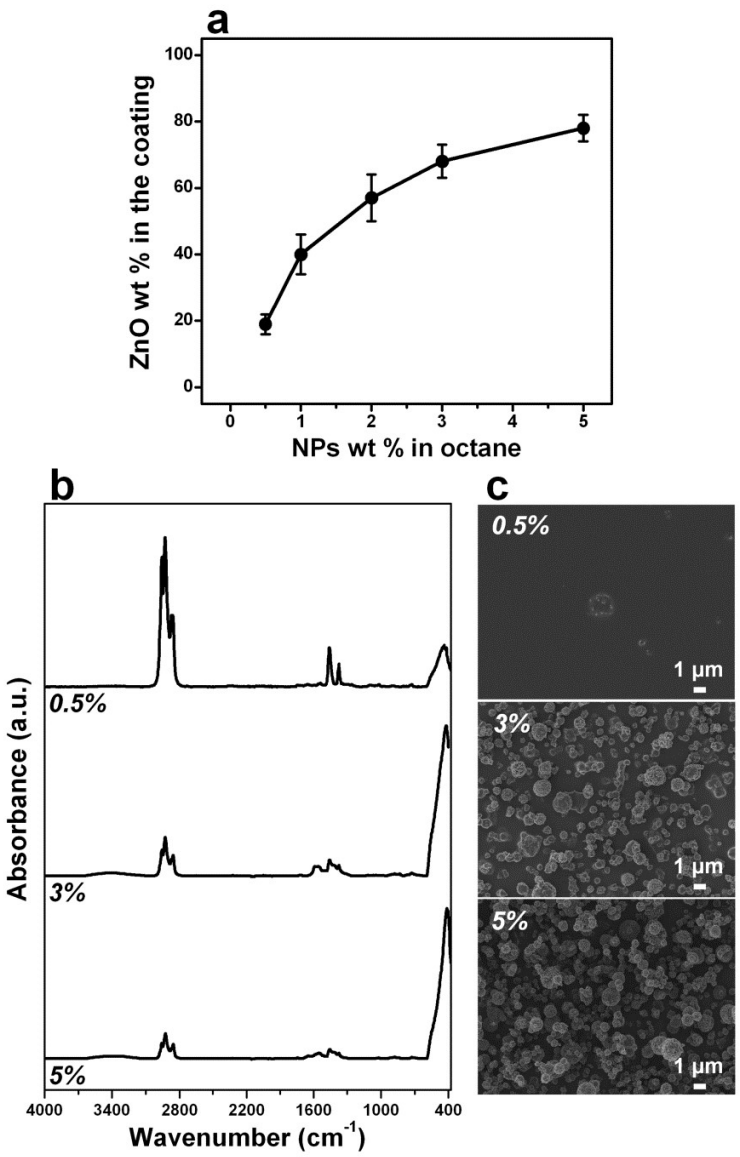

Figure 7. (a) ZnO loading in the NC coating, (b) ATR-FTIR spectra and (c) SEM images of NC coatings deposited by DBD from a dispersion of oleate-capped ZnO NPs in n-octane at a concentration of 0.5, 3 and 5 wt % (deposition time = 10 min).

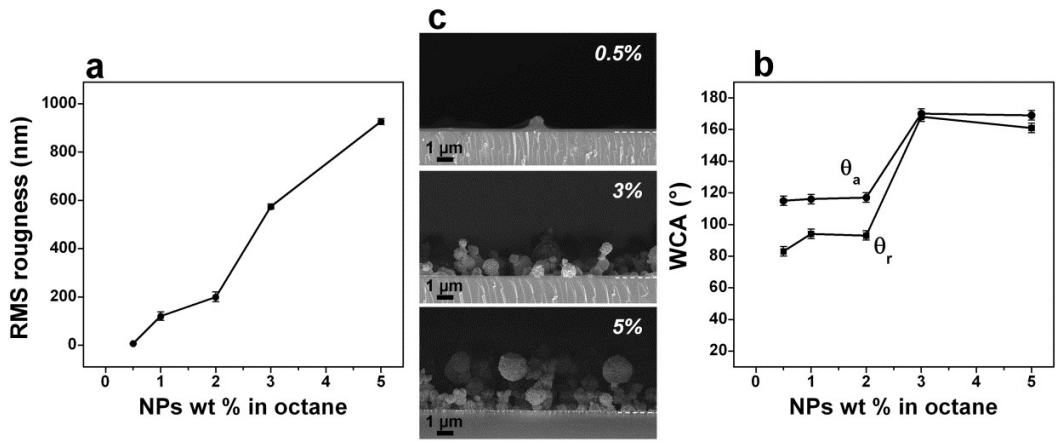

Figure 8. (a) RMS roughness of the NC coatings as a function of the concentration of the oleate-capped ZnO NPs in the dispersion; (b) cross-sectional SEM images of NC films deposited from dispersions at different concentration of the oleate-capped ZnO NPs in n-octane (0.5, 3, 5 wt %); (c) advancing and receding WCAs of the NC coatings as a function of the concentration of the oleate-capped ZnO NPs in the dispersion (deposition time = 10 min).

The detailed investigation of the deposition mechanism in this aerosol-assisted DBD process is beyond the scope of this paper. However, we believe that the mechanism of NC film formation mainly consists of the contemporaneous plasma-polymerization of n-octane and electro-deposition of NPs and NPs agglomerates, even if other contributions cannot be ruled out. The plasma-polymerization of n-octane is due to the formation in the atmospheric plasma of reactive hydrocarbon radicals (e.g., n-octane fragments and oligomeric radicals) from n-octane molecules. In fact, considering the dissociation energies of C-C and C-H bonds in saturated hydrocarbons (~3.6 and ~4.3 eV, respectively), it is reasonable to assume that n-octane molecules undergo fragmentation by collision with energetic electrons (1-10 eV) and He metastable atoms (~20 eV)[39] present in the atmospheric plasma, leading to the formation of reactive hydrocarbon radicals. These radicals are the "true" precursors of the polyethylene-like

polymer, i.e., the building blocks responsible of the growth of the organic component of the NC coating on the surface of the substrate. The electro-deposition (or electro-collection) of NPs and NPs agglomerates is due to the fact that, as reported by Borra et al.,[40,41] NPs and NPs agglomerates can be effectively charged by ions present in the DBD and subsequently collected by the electrodes (i.e., deposited on the substrate located on the electrodes); the charging mechanism and efficiency depend on the particle diameter and on the DBD electrical conditions.[40,41] The fact that the weight percentage of NPs is considerably higher in the NC coatings than in the starting dispersion could be ascribed to an efficient electro-deposition mechanism in the DBD.

Briefly, the main advantage of this deposition process is that it allows the production of an organic-inorganic NC in a single step and at room temperature; importantly, the versatility and generality of this approach mainly resides in the possible combination of a wide range of NPs and in principle of any organic precursor (also an unsaturated hydrocarbon such as n-octane) that introduced in the atmospheric plasma undergo fragmentation and consequent plasma-polymerization.

4. CONCLUSION

In this study a facile atmospheric pressure cold plasma process was developed to deposit, in single step and at room temperature, a novel organic-inorganic hydrocarbon polymer/ZnO nanoparticles nanocomposite coating. Specifically, the synthetic approach involved the utilization of a DBD fed with helium and the aerosol of a dispersion of oleate-capped ZnO nanoparticles in n-octane. It was demonstrated that the deposited nanocomposite coatings present the chemical features of both the oleate-capped ZnO NPs and the polyethylene-like organic

component originated from the plasma-polymerization of n-octane. The coatings contain quasi-spherical nanoparticle agglomerates which promote the formation of a hierarchical surface roughness; the hydrocarbon polymer covers the agglomerates to different extents and seems to contribute to their immobilization in the coating. The increase of both the deposition time and the NPs concentration in the starting dispersion promotes an increase of the ZnO content in the coating, allowing the surface roughness to become less influenced by the morphology of the polymer and more affected by the NPs agglomerates; this ultimately leads to superhydrophobic surfaces with low contact angle hysteresis. Considering the versatility and generality of this deposition method, with particular regard to the possible combination of a wide range of NPs and organic precursors, this study provides a new direction to design and synthesize hierarchical organic-inorganic NC coatings. We are currently investigating the utilization of this NC coatings for photocatalytic, self-cleaning and anti-staining applications as well as the scalability of the deposition process on large-area substrates.

ASSOCIATED CONTENT

Supporting Information

Figure of the plasma reactor, FTIR and XPS spectra of commercial and oleate-capped ZnO NPs, NPs agglomerate size distribution in the NC coating, additional TSEM and SEM images of the ZnO NPs and of the NC coatings, results of the tape peel test. This material is available free of charge via the Internet at http://pubs.acs.org.

AUTHOR INFORMATION

Corresponding Author

* Email: fiorenza.fanelli@cnr.it

Notes

The authors declare no competing financial interest.

ACKNOWLEDGMENT

The research was supported by the Italian Ministry for Education, University and Research (MIUR) under grants PRIN 2009, PON 01_02239 and PONa3_00369, and Regione Puglia under grant no. 51 "LIPP" within the Framework Programme Agreement APQ "Ricerca Scientifica", II atto integrativo - Reti di Laboratori Pubblici di Ricerca. The authors gratefully acknowledge Dr. Antonella Milella for the AFM analyses, Domenico Bedenetti for the ASV measurements, Savino Cosmai and Danilo Benedetti for the skilful technical assistance and Dr. Gianvito Caputo (Department of Chemistry, Humboldt University of Berlin, Germany) for the many valuable discussions.

REFERENCES

(1) Sanchez, C.; Julián, B.; Belleville, P.; Popall, M. Applications of Hybrid Organic–Inorganic Nanocomposites. *J. Mater. Chem.* **2005**, *15*, 3559–3592.

(2) Manca, M.; Cannavale, A.; De Marco, L.; Aricò, A. S.; Cingolani, R.; Gigli, G. Durable Superhydrophobic and Antireflective Surfaces by Trimethylsilanized Silica Nanoparticles-Based Sol-Gel Processing. *Langmuir* **2009**, *25*, 6357–6362.

(3) Manoudis, P. N.; Karapanagiotis, I.; Tsakalof,A.; Zuburtikudis, I.; Panayiotou, C. Superhydrophobic Composite Films Produced on Various Substrates, *Langmuir* **2008**, *24*, 11225–11232.

(4) Steele, A.; Bayer, I.; Loth, E. Inherently Superoleophobic Nanocomposite Coatings by Spray Atomization. *Nano Lett.* **2009**, *9*, 501–505.

(5) Tiwari, M. K.; Bayer, I. S.; Jurisch, G. M.; Schutzius, T. M.; Magaridis, C. M. Highly Liquid-Repellent, Large-Area, Nanostructured Poly(vinylidene fluoride)/Poly(ethyl 2-cyanoacrylate) Composite Coatings: Particle Filler Effects. *ACS Appl. Mater. Interfaces* **2010**, *2*,1114–1119.

(6) Sparks, B. J.; Hoff, E. F. T.; Xiong, L.; Goetz, J. T.; Patton, D. L. Superhydrophobic Hybrid Inorganic−Organic Thiol-ene Surfaces Fabricated via Spray-Deposition and Photopolymerization. *ACS Appl. Mater. Interfaces* **2013**, *8*, 1811–1817.

(7) Raza, A.; Si, Y.; Wang, X.; Ren, T.; Ding, B.; Yu, J.; Al-Deyabd, S. S. Novel Fluorinated Polybenzoxazine–Silica Films: Chemical Synthesis and Superhydrophobicity. *RSC Adv.* **2012**, *2*, 12804–12811.

(8) Palgrave, R. G.; Parkin, I. P. Aerosol Assisted Chemical Vapor Deposition Using Nanoparticle Precursors: A Route to Nanocomposite Thin Films. *J. Am. Chem. Soc.* **2006**, *128*, 1587–1597.

(9) Hou, X.; Choy, K.-L. Processing and Applications of Aerosol-Assisted Chemical Vapor Deposition. *Chem. Vap. Dep.* **2006**, *12,* 583–596.

(10) Crick, C. R.; Bear, J. C.; Kafizas, A.; Parkin, I. P., Superhydrophobic Photocatalytic Surfaces through Direct Incorporation of Titania Nanoparticles into a Polymer Matrix by Aerosol Assisted Chemical Vapor Deposition. *Adv. Mater.* **2012**, *24*, 3505–3508.

(11) Crick, C. R.; Bear, J. C.; Southern, P.; Parkin, I. P. A General Method for the Incorporation of Nanoparticles into Superhydrophobic Films by Aerosol Assisted Chemical Vapour Deposition. *J. Mater. Chem. A* **2013**, *1*, 4336–4344.

(12) Fanelli, F.; Fracassi, F. Aerosol-assisted atmospheric pressure plasma deposition of organic-inorganic NC coatings. *Plasma Chem. Plasma Process.* Accepted.

(13) Bardon, J.; Bour, J.; Del Frari, D.; Arnoult, C.; Ruch, D. Dispersion of Cerium-Based Nanoparticles in an Organosilicon Plasma Polymerized Coating: Effect on Corrosion Protection. *Plasma Process. Polym.* **2009**, *6*, S655–S659.

(14) Michel, M.; Bour, J.; Petersen, J.; Arnoult, C.; Ettingshausen, F.; Roth, C.; Ruch D. Atmospheric Plasma Deposition: A New Pathway in the Design of Conducting Polymer-Based Anodes for Hydrogen Fuel Cells. *Fuell Cells* **2010**, *10*, 932–937.

(15) Dowling, D.P.; Twomey, B.; Byrne, G. Effect of Titanium Oxide Nanoparticle Incorporation into nm Thick Coatings Deposited Using an Atmospheric Pressure Plasma. *J. Nanosci. Nanotechnol.* **2010**, *10*, 2746–2752.

(16) Dembele, A.; Rahman, M.; Reid, I.; Twomey, B.; Don MacElroy, J. M.; Dowling, D. Deposition of Hybrid Organic–Inorganic Composite Coatings Using an Atmospheric Plasma Jet System. *J. Nanosci. Nanotechnol.* **2011**, *11*, 1–8.

(17) Uygun, A.; Oksuz, L.; Yavuz, A. G.; Guleç, A.; Sen, S. Characteristics of Nanocomposite Films Deposited by Atmospheric Pressure Uniform RF Glow Plasma. *Curr. Appl. Phys.* **2011**, *11*, 250–254.

(18) Beamson, G.; Briggs, D. *High Resolution XPS of Organic Polymers*; J. Wiley & Sons: Chichester, 1992.

(19) Sethi, S.; Dhinojwala, A. Superhydrophobic Conductive Carbon Nanotube Coatings for Steel. *Langmuir* **2009**, *25*, 4311–4313.

(20) Lee, S.-M.; Kim, K.-S.; Pippel, E.; Kim. S.; Kim J.-H.; Lee H.-J. Facile Route Toward Mechanically Stable Superhydrophobic Copper Using Oxidation−Reduction Induced Morphology Changes. *J. Phys. Chem. C* **2012**, *116*, 2781−2790.

(21) Fanelli, F.; Fracassi, F.; d'Agostino, R. Deposition of Hydrocarbon Films by Means of Helium-Ethylene Fed Glow Dielectric Barrier Discharges. *Plasma Process. Polym.* **2005**, *2*, 688–694.

(22) Zhang, L.; Yin, L.; Wang, C.; Lun, N.; Qi, Y. Sol-Gel Growth of Hexagonal Faceted ZnO Prism Quantum Dots with Polar Surfaces for Enhanced Photocatalytic Activity. *ACS Appl. Mater. Interfaces* **2010**, *2*, 1769–1773.

(23) Yang, M.; Yin, G.; Huang, Z.; Kang, Y.; Liao, X.; Wang, H. Preparation and Optical Properties of Biomimic Hierarchical ZnO Column Arrays. *Cryst. Growth Des.* **2009**, *9*, 707–714.

(24) Deacon, G. B.; Phillips, R. J. Relationships between the Carbon-Oxygen Stretching Frequencies of Caboxylato Complexes and the Type of Carboxylate Coordination. *Coord. Chem. Rev.* **1980**, *33*, 227–250.

(25) Lu, Y.; Miller, J. D. Carboxyl Stretching Vibrations of Spontaneously Adsorbed and LB-Transferred Calcium Carboxylates as Determined by FTIR Internal Reflection Spectroscopy. *J. Coll. Interf. Sci.* **2002**, *256*, 41–52.

(26) Patel, J. D.; Mighri, F.; Ajji, A. Generalized Chemical Route to Develop Fatty Acid Capped Highly Dispersed Semiconducting Metal Sulphide Nanocrystals. *Mat. Res. Bull.* **2012**, *47*, 2016–2021.

(27) Liu, D.; Wu, W.; Qiu, Y.; Yang, S.; Xiao, S.; Wang, Q.-Q.; Ding, L.; Wang, J. Surface Functionalization of ZnO Nanotetrapods with Photoactive and Electroactive Organic Monolayers. *Langmuir* **2008**, *24*, 5052–5059.

(28) Barreca, D.; Gasparotto, A.; Maccato, C.; Maragno, C.; Tondello, E. ZnO Nanoplatelets Obtained by Chemical Vapor Deposition, Studied by XPS. *Surf. Sci. Spectra* **2007**, *14*, 19–26.

(29) Barreca, D.; Ferrucci, A. P.; Gasparotto, A.; Maccato, C.; Maragno, C; Tondello, E. Temperature-Controlled Synthesis and Photocatalytic Performance of ZnO Nanoplatelets. *Chem. Vap. Dep.* **2007**, *13,* 618–625.

(30) Bekermann, D.; Gasparotto, A.; Barreca, D.; Bovo, L.; Devi, A.; Fischer, R. A.; Lebedev, O. I.; Maccato, C.; Tondello, E.; Van Tendeloo, G. Highly Oriented ZnO Nanorod Arrays by a Novel Plasma Chemical Vapor Deposition Process. *Cryst. Growth Des.* **2010**, *10*, 2011–2018.

(31) Pradhan, D.; Leung, K. T. Controlled Growth of Two-Dimensional and One-Dimensional ZnO Nanostructures on Indium Tin Oxide Coated Glass by Direct Electrodeposition. *Langmuir* **2008**, *24*, 9707–9716.

(32) Lind, A.; du Fresne von Hohenesche, C.; Smatt, J.-H.; Lindén, M.; Unger, K. K. Spherical Silica Agglomerates Possessing Hierarchical Porosity Prepared by Spray Drying of MCM-41 and MCM-48 Nanospheres. *Microp. Mesop. Mater.* **2003**, *66*, 219–227.

(33) Iskandar, F.; Chang, H.; Okuyama, K. Preparation of Microencapsulated Powders by an Aerosol Spray Method and their Optical Properties. *Adv. Powd. Technol.* **2003**, *14*, 349–367.

(34) Lee, S. G.; Ham, D. S.; Lee, D. Y.; Bong, H.; Cho, K. Transparent Superhydrophobic/Translucent Superamphiphobic Coatings Based on Silica−Fluoropolymer Hybrid Nanoparticles. *Langmuir* **2013**, *29*, 15051−15057.

(35) Hou, X.; Choy, K.-L.; Brun, N.; Serín, V. Nanocomposite Coatings Codeposited with Nanoparticles Using Aerosol-Assisted Chemical Vapour Deposition. *J. Nanomater.* **2013**, *2013*, 219039.

(36) Goldstein, J.; Newbury, D.; Joy, D.; Lyman, C.; Echlin, P.; Lifshin, E.; Sawyer, L.; Michael, J. *Scanning Electron Microscopy and X-ray Microanalysis (3rd edition)*; Springer Science + Business Media: New York, 2003.

(37) Klein, T.; Buhr, E.; Frase, C. G. TSEM: a Review of Scanning Electron Microscopy in Transmission Mode and Its Applications. In *Advances in Imaging and Electron Physics*; Awakes, P., Ed. Academic Press: New York, 2012; Vol. 171, pp. 297–356.

(38) Yüce, M. Y.; Levent Demirel, A.; Menzel, F. Tuning the Surface Hydrophobicity of Polymer/Nanoparticle Composite Films in the Wenzel Regime by Composition. *Langmuir* **2005**, *21*, 5073–5078.

(39) Massines, F.; Sarra-Bournet, C.; Fanelli, F.; Naudé, N.; Gherardi, N. Atmospheric Pressure Low Temperature DirectPlasma Technology: Status and Challenges for Thin Film Deposition. *Plasma Process. Polym.* **2012**, *9*, 1041–1073.

(40) Borra, J.P. Nucleation and aerosol processing in atmospheric pressure electrical discharges: powders production, coatings and filtration. *J. Phys. D Appl. Phys.* **2006**, *39,* R19–R54.

(41) Borra, J.P. Charging of aerosol and nucleation in atmospheric pressure electrical discharges. *Plasma. Phys. Control. Fusion* **2008**, 50,124036.

TOC GRAPHIC